Study on Kinetics of Polymer Melt Intercalation by a Rheological Approach

Jian Li,[1] Chixing Zhou,[1] Gang Wang,[1] Delu Zhao[2]

[1]*School of Chemistry and Chemical Technology, Shanghai Jiaotong University, Shanghai 200240, China*
[2]*Institute of Chemistry, The Chinese Academy of Science, Beijing 100080, People's Republic of China*

Received 30 May 2002; accepted 13 September 2002

ABSTRACT: The kinetics of melt intercalation of poly(propylene)/montmorillonite nanocomposites was studied by a rheological approach. The experimental sample was elaborately prepared to investigate the whole intercalating process. The intercalation process was demonstrated by the changes of the viscoelastic response with annealing time. The development of the relative volume fraction of intercalated tactoids was obtained from the rheological characterization. The apparent diffusivities was determined and the activation energy of melt intercalation was found to be about 80 ± 6 kJ/mol. © 2003 Wiley Periodicals, Inc. J Appl Polym Sci 89: 318–323, 2003

Key words: nanocomposites; kinetics; polypropylene

INTRODUCTION

Nanocomposites based on organic polymers and inorganic clay minerals consisting of silicate layers (PSLN) such as montmorillonite (MMT) have attracted great interest to researchers as a new means to develop advanced polymer composites. A large number of polymer–clay nanocomposites have been successfully synthesized through incorporating clay in various polymer matrixes such as polyamide,[1–3] polyimide,[4] epoxy resin,[5,6] phenolic resin,[7] polyurethane,[8] polystyrene,[9] poly(propylene),[10–12] poly(butyleneterephthalate)[13] and so on. They frequently exhibit the dramatic enhancements in their physical, thermal, gas barrier, and mechanical properties with the relative low inorganic loading required. Several strategies, such as *in situ* intercalation polymerization, exfoliation adsorption[14] and melt intercalation, have been developed to fabricate polymer/clay nanocomposites. Among these strategies, the melt intercalation is attractive because of its versatility, its compatibility with current polymer processing techniques, and its environmentally benign character due to the absence of solvent. In the progress of melt intercalation, the layered silicate is mixed with the polymer matrix in the molten state, and the polymer chains crawl into the interlayer space and form either an intercalated or an exfoliated nanocomposites. As far as the melt intercalation is concerned, the kinetics of the progress, i.e., how polymer chain diffuse into the galleries of the silicate layers, is one of the most important questions from the point of both industrial and scientific view. Vaia et al.[15] have studied the kinetics of polymer melt intercalation in polystyrene (PS)/organically modified fluorohectorite hybrids mainly by wide-angle X-ray diffraction (WAXD) and transmission electron microscope (TEM). They found that PS melt intercalation in organically modified mica-type silicate is controlled by mass transport into the primary particles of the silicate and is not specifically limited by diffusion of the polymer chains within the silicate gallery. The activation energy of hybrid formation is similar to that of the PS self-diffusion in the bulk melt. A further study on the intercalation kinetics of PS/synthetic 2 : 1 layered silicate hybrids was conducted by Manias et al.[16] to explore the influence of molecular weight and polymer–surface interaction on the diffusion with the *in situ* small-angle neutron scattering (SANS) and intermediate-angle neutron scattering (LANS) besides the WAXD method.

It has been found that the linear viscoelastic response of polymer/silicate nanocomposites to the small amplitude oscillatory shear (SAOS) is quite different from that of the polymer matrix. For example, compared with that of the polymer matrix, the storage dynamic modulus (G') of nanocomposites enhances remarkably at the low frequencies.[17] Therefore, it is feasible to monitor the microstructural evolution by using some rheological parameterd such as modulus and viscosity as the indicators. Galgali et al.[13] studied the changes of elastic and loss modulus of PP/MMT hybrids as a function of annealing time to investigate

Correspondence to: C. Zhou (cxzhou@mail.sjtu.edu.cn).
Contract grant sponsor: the Special Funds for Major State Basic Research Projects; contract grant number: G199906408.
Contract grant sponsor: National Natural Science Foundation of China; contract grant number: 20174024.

Journal of Applied Polymer Science, Vol. 89, 318–323 (2003)
© 2003 Wiley Periodicals, Inc.

the microstructural changes in PP/MMT hybrids. But limited by the experimental method, they did not actually explore the intercalating process in the rheometer because the intercalation in their experimental samples produced by extruder had almost completed before the rheological characterization. In this communication, we intend to present a rheological approach to investigate the microstructural evolution and the intercalation kinetics of the PP/MMT hybrids. To achieve this goal, it is necessary to improve the preparation of the samples for the experiment. Therefore, we developed an elaborate method to prepare the samples, which is described in the experimental section later.

EXPERIMENTAL

Materials

Poly(propylene) (PP, grade Montell 5C39F) of M_w = 300,000 was used as the matrix. Additive-free low isotactic homopolypropylene elastomer (LiPP) of M_w = 106,000 determined by high temperature GPC (Water-150C, America) and isotacticity of 0.47 determined by by ^{13}C NMR (Bruker-AM300, Switzerland) was generously provided by Research Institute of Yanshan Petrochemical Co. Maleic anhydride (MAH) grafted low isotactic homopolypropylene elastomer (LiPP-*g*-MAH) containing 0.36 wt % MAH was prepared in our laboratory by solid-phase grafting. The commercial organic montmorillonite, MMT908A, modified with alkyl ammonium was supplied by Huate Co., Zhejiang Province, China.

Sample preparation

PP and MMT908A was premixed to fabricate PP/MMT908A composite, where the loading of MMT908A was 9 wt %. Then the composite and LiPP-*g*-MAH were compressed into films with the thickness of 0.4 mm at 190°C, respectively. Four PP/MMT908A and three LiPP-*g*-MAH films were alternatively superposed and compressed into a laminated sheet with the thickness of 1 mm at about 140°C. Because LiPP-*g*-MAH has a broad melting rang, from 80–160°C, the resulted sheet is composed of four pieces of PP/MMT films adhered together by three pieces of LiPP-*g*-MAH films that was also used as the intercalation agent. Hereafter, such a multilayered sample is referred to as the PP/908A blend.

Rheometry

Rheological measurements were carried out in a small amplitude oscillatory frequency sweep mode on a rheometer (ARES rheometer, Rheometrics Scientific, NJ) equipped with a parallel plate geometry using 25 mm-diameter plates. All measurements were performed with a 200 FRTN1 transducer at a lower resolution limit of 0.02 g · cm. The sample was annealed for several hours at a predetermined temperature in the rheometer in a nitrogen environment, and during the annealing period the frequency sweep was carried out about every 8-min interval. All the sweeps were conducted at a strain of 0.1%.

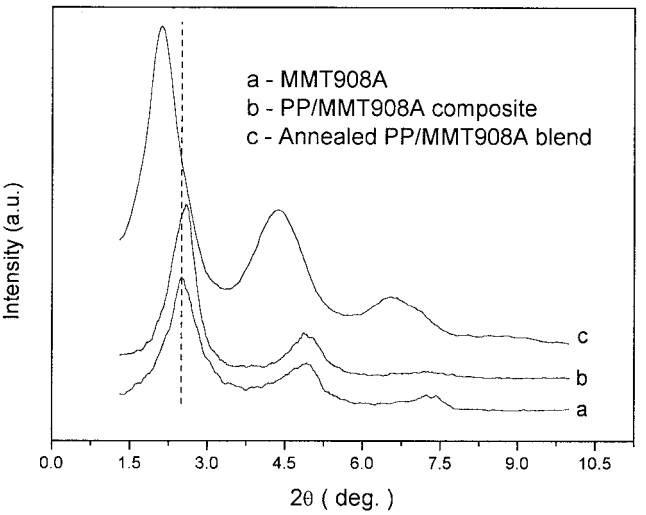

Figure 1 WAXD patterns of MMT908A, the PP/MMT908A composite, and the annealed PP/MMT908A blend.

WAXD

The X-ray diffraction experiments were performed on a Rigaku Dmax-rC diffractometer with a Cu target and a rotating anode generator operated at 40 kV and 100 mA. Samples were scanned from 1.5 to 10° at the rate of 2°/min.

Figure 1 shows WAXD patterns for MMT908A, the PP/MMT908A composite, and the PP/MMT908A blend annealed for 6 h in the rheometer at 200°C. The interlayer distances of silicates for pure MMT908A, the PP/MMT908A composite, and the annealed blend, which can be calculated out from the d_{001} peak obtained by WAXD, are 3.53, 3.40, and 4.10 nm, respectively. It elucidates that in the PP/MMT908A composites there was no PP chain crawl into the interlayers of MMT908A, and the decrease of the interlayer spacing may come from the thermal decomposition and release of organic surfactants that reside in the gallery of silicate layers. For the annealed blend, the d_{001} distance expands to 4.10 nm, which confirms that intercalation happened during annealing.

TEM

The ultrathin sections of samples with a thickness of 100 nm were prepared at −80°C using a cryoultrami-

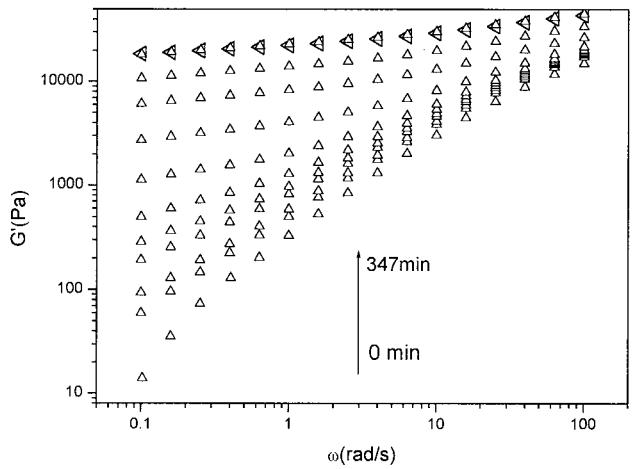

(a)

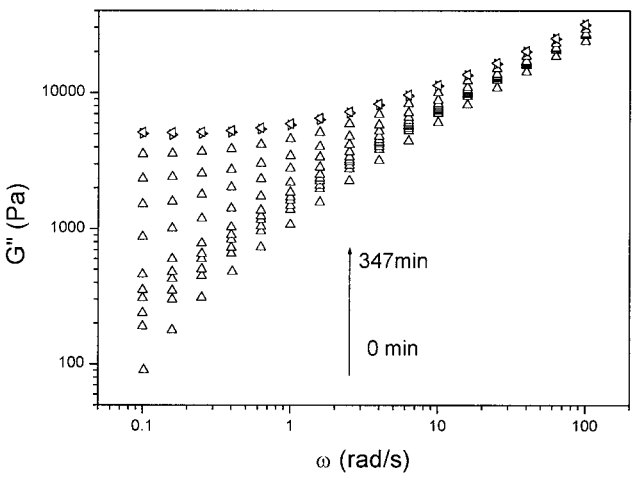

(b)

Figure 2 Development of dynamic modulus (a) storage modulus and (b) loss modulus with annealing time.

crotome (LKB 2088, Sweden). The transmission electron micrographs were taken from these sections using a transmission electron microscope (HITACHI H-860, Japan) with a 100-kV accelerating voltage.

RESULTS AND DISCUSSION

The development of the linear viscoelastic response with the annealing time was recorded by the rheometer. Figure 2(a) and (b) show the time evolution of the elastic modulus (G') and the loss modulus (G'') during annealing at 200°C, respectively. As shown in Figure 2, it is fount that the viscoelastic response to SAOS changed continuously until annealing for about 6 h. Here it may be suggested that all the microstructural evolution have been finished if the viscoelastic response does not change with annealing time. At the beginning, the sample showed a near-terminal behavior (G'–ω^2, G''–ω), which indicated that initially the viscoelastic response to the SAOS was dominated by the matrix. With increasing of the annealing time, G' and G'' increased monotonically. It is notable that G' and G'' were continuously increasing and became gradually independent of ω at the low frequencies, but G' increased faster than G''. The distinct change was also observed for the dynamic viscosity (η), which increased considerably and finally displayed a distinct shear-thinning behavior at low frequencies as shown in Figure 3. It is believed that the deviation of the viscoelastic behavior from the linear viscoelastic terminal behavior at low frequencies is the clue of intercalation process. It can be thought that polymer chains intercalated into silicate interlayers must be confined between parallel walls separated by a distance smaller than or of the same order of the size of the chain coils. The confinement effect may lead to the change of the relaxation dynamics of polymer, which seems to be able to explain the increase in low-frequency modulus and viscosity. However, it has been proven that the solid-like rheological response at low frequencies does not arise from confinement of chains, and it is extensively accepted that the low-frequency solid-like behaviors come from the formation of percolation networks,[13] which can be also observed in traditional high-filled polymer composites. In percolation system, one of the most important parameters is the critical percolation volume fraction or percolation threshold, ϕ^*. When the volume fraction of filler, ϕ, is above ϕ^*, the three-dimensional filler–filler network structures form. As can be seen in Figure 3(a), it is observed the gradual transition from linear viscoelastic system to percolation one with increasing the annealing time. Taking into account that the size and shape of fillers have great effect on the percolation limit, the forma-

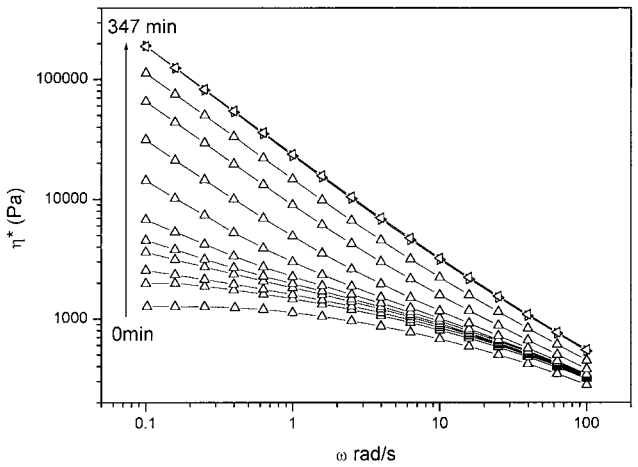

Figure 3 Development of dynamic viscosity with annealing time.

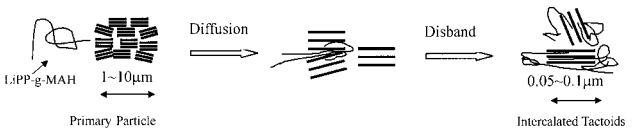

Figure 4 Schematic depicting of the microstructural evolution during intercalation.

tion of a percolation network during annealing is indicative of microstructural changes during annealing of the sample. It has been reported that ϕ^* is quite sensitive to the shapes of filler, and the value of ϕ^* of platelet-type fillers is much smaller than that of sphere-type ones.[18] Therefore, we can image the evolution of the microstructure during annealing as schematically represented in Figure 4. The highly anisotropic platelet-like tactoids composed of several tens of silicate layers are tightly packed to form the so-called primary particles with the size of 1–10 μm,[19] due to the strong interaction between tactoids with large specific surface area. During the annealing process, the chains of LiPP-*g*-MAH penetrate the primary particle from the exterior melts through slits between the tactoids. The penetrated chains then intercalate into interlayers of the tactoids. The intercalated tactoids may disperse into the matrix due to the decrease of both the interfcial tension between them and the matrix and the interaction between themselves. The intercalated tactoids dispersing in the matrix was observed by TEM as shown in Figure 5.

Because of their highly geometric anisotropy and larger interfacial area, the effects of tactoids on the viscoelastic response are much greater than the primary particles. As seen in Figures 2 and 3, the enhancement of modulus and viscosity resulted from the increasing tactoids detached from the primary particles with intercalation proceeding. It is distinct that the low-frequency modulus and viscosity have strong dependence on the volume fraction of detached tactoids, $\phi(t)$, the value of which is increasing with annealing time. There is a good approximation for η over the volume fraction range of $0 < \phi(t) < \phi^*$ as follows:[18]

$$\frac{\eta_d(t)}{\eta_m} = \left(1 - \frac{\phi(t)}{\phi^*}\right)^{-2} \tag{1}$$

where η_m and $\eta_d(t)$ is the zero-shear viscosity of the matrix fluid and the zero-shear viscosity of the tactoid-dispersing fluid respectively. Additionally, here the formation of percolation network or physical jamming is indicated by $G' > G''$ in the frequency range of $10^{-2} < \omega < 10^0$ Hz.[20] For example, annealed at 200°C, the physical jamming happened at the annealing time of 60 min. Because the percolation network does not form and the shear-thinning behavior is not distinct at the low frequecies yet, it is assumed that the Cox-Merz rule is still valid, and the viscosity measured at $\omega = 0.1$ rad/s is used as the zero-shear viscosity. Using eq. (1), the ratio of $\phi(t)$ to ϕ^* can be determined by the data of $\eta(t)$ before the physical jamming. After the formation of percolation networks or physical jamming, ($\phi(t) > \phi^*$), the liquid-like behavior may transit into the solid-like one, and G' at low frequency may increase approximately in a power law manner with $\phi(t)$ as follows:[21]

$$G'(t) = G'_{\text{gel}}\left(\frac{\phi(t)}{\phi^*}\right)^s \tag{2}$$

where G'_{gel} is the modulus measured at the beginning of percolation formation ($\phi(t) = \phi^*$), the value of s is reported to be near 4.9. Because $G'(t)$ was shown to be weakly dependent on ω at low frequencies after the physical jamming, we suggest $G'(t)$ values measured at $\omega = 0.1$ rad/s as the low-frequency plateau G'. Because the accomplishment of intercalation can be indicated by the invariable viscoelastic response to SAOS with annealing time, the ratio of the terminal volume fraction of intercalated tactoids, $\phi(\infty)$, to ϕ^*, was determined by the G' data from the final invariable viscoelastic response by using eq. (2). Therefore, the ratio of $\phi(t)$ to ϕ^*, from the formation of percolation network to the accomplishment of intercalation, can be obtained from the $G'(t)$ data by using eq. (2). Finally, combining the results of $\phi(t)/\phi^*$ before and after physical jamming, the development of the volume fraction ratio, $\phi(t)/\phi^*$, with annealing time in the whole intercalation process can be obtained. Further, dividing $\phi(t)/\phi^*$ by $\phi(\infty)/\phi^*$, the relative volume fraction of the intercalated tactoids, $\phi(t)/\phi(\infty)$, can be determined with no need of the specific value of ϕ^*, which may be considerably obscure for the nanocom-

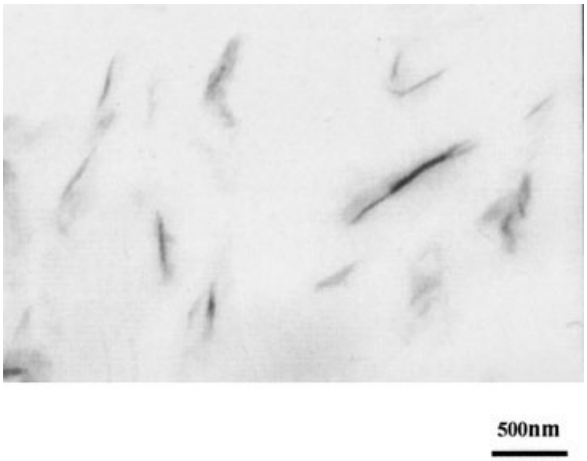

Figure 5 TEM image of the PP/MMT908A blend annealed at 200°C for 6 h at 20,000 magnification.

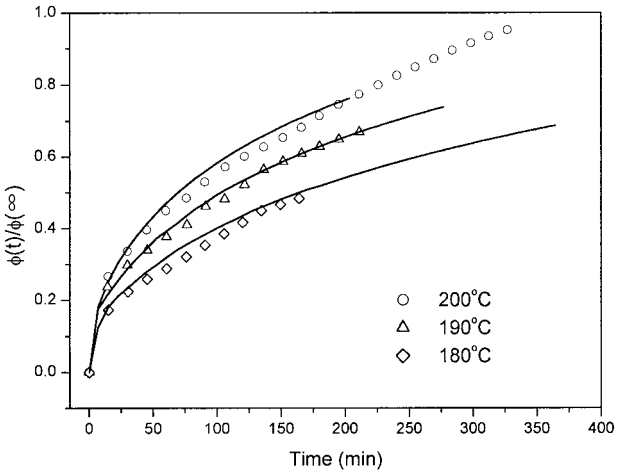

Figure 6 Relative volume fractions of intercalated tactoids as a function of annealing time at 200, 190, and 180°C. Solid lines are best fits to the data using eq. (3).

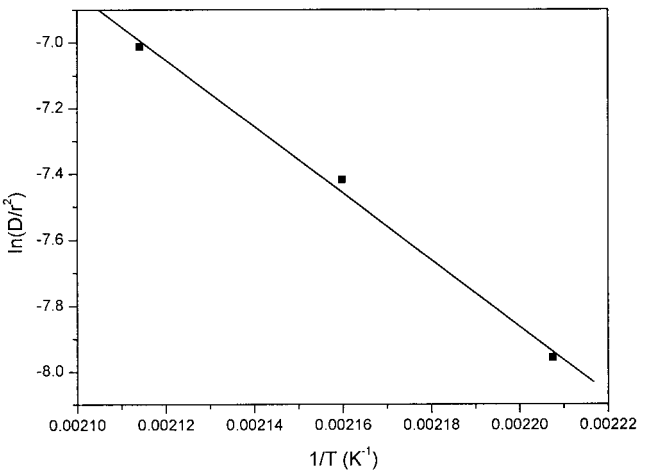

Figure 7 Plot of $\ln(D/r^2)$ vs. $1/T$. The activation energy of melt intercalation is determined from the slop of the fitting line.

posites. Figure 6 shows the resulted value of $\phi(t)/\phi(\infty)$ developing with annealing time.

Assuming that the melt intercalation is limited by mass transport of LiPP-*g*-MAH into the primary particles, which may be described as a Ficken process with a single, apparent, concentration independent diffusivity, D, the ratio of the amount of polymer diffused into primary particles, $Q(t)$, to that at equilibrium, $Q(\infty)$ is:[15,23]

$$\frac{Q(t)}{Q(\infty)} = 1 - \sum_{m=1}^{\infty} \frac{4}{\alpha_m^2} \exp\left(- \frac{D}{r^2} \alpha_m^2 t \right) \qquad (3)$$

where D/r^2 is the effective diffusivity, r is the mean radius of the primary particle, and α_m is the mth positive root of the zeroth-order Bessel function ($J_0(\alpha) = 0$). Considering that the volume fraction of intercalated tactoids, $\phi(t)$, is corresponding to the amount of polymer diffused into primary particles, $Q(t)$, the value of $Q(t)/Q(\infty)$ can be given by the corresponding relactive volume fraction of the intercalated tactoids, $\phi(t)/\phi(\infty)$. As seen in Figure 6, the experimental data were fit using eq. (3) to obtain the value of D/r^2 at different annealing temperature. Assuming that r is approximately 5 μm, the apparent diffusivities, D, can determined from the effective diffusional rates, and the results are listed in Table I. Furthermore, assuming the effective diffusivity has an Arrhenius temperature dependence, the activation energy of melt intercalation of LiPP-*g*-MAH in 908A, $\Delta E_{\eta 0}$, is approximately 84 ± 6 kJ/mol, which can be obtained by plotting ln D/r^2 vs. $1/T$ as shown in Figure 7. Because the self-diffusion coefficient D_0 scales with T/η_0^{23} where η_0 is the zero-shear viscosity and also has an Arrhenius temperature dependence, the value of the activation energy of self-diffusion ΔE_{D0} may be quite close to that of zero-shear viscosity, $\Delta E_{\eta 0}$ (55 ± 5 kJ/mol). Comparaing ΔE_D with $\Delta E_{\eta 0}$ shows that ΔE_D is a bit larger than $\Delta E_{\eta 0}$. It seems to indicate that the activation energy of melt intercalation is larger than that of the self-diffusion of LiPP but in the same order, which may result from the interactions of MAH grafted LiPP chains and the polar silicate surface.

TABLE I
The Values of the Effective Diffusivity and Apparent Diffusivity at Different Temperatures

	180°C	190°C	200°C
D/r^2 (1/s)	0.00035	0.00061	0.00090
D (cm^2/s)	8.8×10^{-13}	1.5×10^{-12}	2.2×10^{-12}

CONCLUSIONS

The melt intercalation kinetics of PP/MMT nanocomposites was studied by a rheological approach. To observe the whole intercalating process, the experimental sample was deliberately designed to be made up of four films of PP/MMT blend and three films of LiPP-*g*-MAH, which were alternatively superimposed to compress into a sheet. By recording the change of vicsoelastic response to SAOS, it was found that the increasing of intercalated tactoids detached from the primary particles resulted in the continuous enhancement of low-frequency modulus and viscosity and the formation of the percolation networks. The development of the relative volume fraction of intercalated tactoids was obtained from the rheological parameters of viscosity and storage modulus, which could be used to determine the apparent diffusivities for mass transport into the

primary particles at the different temperatures. The activation energy of melt intercalation was found to be about 80 ± 6 kJ/mol.

References

1. Kojima, Y.; Usuki, A.; Kawasumi, M.; Okada, A.; Kurauchi, T.; Kamigaito, O. J Polym Sci Part A Polym Chem 1993, 31, 983.
2. Wu, Z. G.; Zhou, C. X.; Qi, R. R.; Zhang, H. B. J Appl Polym Sci 2002, 83, 2403.
3. Wu, Z. G.; Zhou, C. X. Polym Testing 2002, 21, 479.
4. Tyan, H. L.; Liu, Y. C.; Wei, K. H. Chem Mater 1999, 11, 1942.
5. Lan, T.; Pinnavaia, T. J. Chem Mater 1994, 6, 2216.
6. Kornmann, X.; Lindberg, H.; Bergluad, L. A. Polymer 2001, 42, 4493.
7. Wu, Z. G.; Zhou, C. X.; Qi, R. R. Polym Compos 2002, 23, 634.
8. Chen, T. K.; Yi, T.; Wei, K. H. J Polym Sci Part A Polym Chem 1999, 37, 2225.
9. Vaia, R. A.; Jandt, K. D.; Kramer, E. J.; Giannelis, E. P. Chem Mater 1996, 8, 2628.
10. Kawasumi, M.; Hasegawa, N.; Kato, M.; Usuki, A.; Okada, A. Macromolecules 1997, 30, 6333.
11. Usuki, A.; Kato, M.; Okada, A.; Kurauchi, T. J. J Appl Polym Sci 1997, 63, 137.
12. Galgali, G.; Ramesh, C.; Lele, A. Macromolecules 2001, 34, 852.
13. Li, X. C.; Kang, T.; Cho, W. J. Lee, J. K.; Ha, C. S. Macromol Rapid Commun 2001, 21, 1040.
14. Alexander, M.; Dubois, P. Mater Sci Eng 2000, 28, 1.
15. Vaia, R. A.; Jandt, K. D.; Kramer, E. J.; Giannelis, E. P. Macromolecules 1995, 28, 8080.
16. Manias, E.; Chen, H.; Krishnamoorrti, R.; Genzer, J.; Kramer, E. J.; Giannelis, E. P. Macromolecules 2000, 33, 7955.
17. Solomon, M. J.; Almusallam, A. S.; Seefeldt, K. F.; Somwangthanaroj, A.; Varadan, P. Macromolecules 2001, 34, 1864.
18. Bicerano, J.; Douglas, K. F.; Brune, D. A. J Polym Sci Part C Rev Macromol Chem Phys 1999, 39, 561.
19. Wu, Z. G. PhD Thesis, Shanghai Jiaotong University, China.
20. Yanez, J. A.; Laarz, E.; Bergstrom, L. J Colloid Interface Sci 1999, 209, 162.
21. Rueb, C. J.; Zukoski, C. F. J Rheol 1997, 41, 212.
22. Breen, C.; Deane, T.; Flynn, J. J.; Reynolds, D. Clays Miner 1987, 35, 336.
23. Gell, C. B.; Graessley, W. W.; Fetters, L. J. J Polym Sci Part B Polym Phys 1997, 35, 1933.